Solution Structure of the Satiety Factor, CART, Reveals New Functionality of a Well-Known Fold†

Svend Ludvigsen,* Lars Thim, Ane M. Blom, and Birgitte S. Wulff

Novo Nordisk A/S, Novo Allé 1, DK-2880 Bagsvaerd, Denmark

Received March 2, 2001; Revised Manuscript Received June 5, 2001

ABSTRACT: Cocaine and amphetamine regulated transcript (CART) peptide has been shown to be an anorectic peptide that inhibits both normal and starvation-induced feeding and completely blocks the feeding response induced by neuropeptide Y and regulated by leptin in the hypothalamus. The C-terminal part containing the three disulfide bridges CART(48−89) is the biologically active part of the molecule affecting food intake. The solution structure of the active part of CART has a fold equivalent to other functionally distinct small proteins. CART consists mainly of turns and loops spanned by a compact framework composed by a few small stretches of antiparallel β-sheet common to cystine knots.

The hypothalamic peptide cocaine and amphetamine regulated transcript (CART)[1] has recently been described as being a new anorectic peptide regulated by leptin (*1*). ICV injections of recombinant CART inhibits both normal and starvation-induced feeding, and completely blocks the feeding response induced by neuropeptide Y (*1*). CART thus belongs to a growing family of brain peptides involved in appetite regulation (*2*).

CART was originally described as an mRNA induced in the brain after acute administration of cocaine to rats (*3*). The rat CART cDNA encodes a peptide of either 129 or 116 amino acid residues in length (*4*). The predicted leader sequence is 27 amino acid residues, thus resulting in a mature CART peptide consisting of either 102 (long form) or 89 (short form) amino acid residues (*4*). In contrast to the rat, only the short form exists in humans (*4*). The mature peptide contains several potential cleavage sites (mono- and dibasic sequences), and CART is posttranslationally processed in vivo into several biologically active fragments (*5*). Posttranslational processing at a Lys 40−Arg 41 sequence in the middle of the 89-residue human peptide generates an N-terminal peptide of 39 amino acids, CART(1−39), and a C-terminal peptide of 48 residues, CART(42−89), and the corresponding processing in the 102-residue rat peptide generates CART(1−52) and CART(55−102). The human CART(42−89) is identical to the rat CART(55−102) except for the N-terminal residue, which is Val in the human peptide and Ile in the rat peptide. This C-terminal peptide has been isolated from hypothalamus, nucleus accumbens, and anterior lobe of pituitary from the rat (*5*), and this form probably corresponds to the peptide that was isolated from ovine hypothalamic extracts by Spiess and co-workers (*6*) in the eighties. In addition, a shorter C-terminal form, CART(49−89), was isolated from rat hypothalamus, nucleus accumbens, and neurointermediate and posterior lobe of pituitary (*5*).

From a peripheral tissue, rat adrenal gland, only full-length CART(1−89) or almost full-length CART(10−89) could be isolated (*5*), indicating that the CART precursor is differentially processed in central and peripheral tissues from the rat. A number of CART peptides, starting at positions 41, 42, 48, and 49 and ending at position 89, have all been produced by recombinant technology in yeast and shown to inhibit food intake when injected ICV in mice (*5*). These results demonstrate that the C-terminal part containing the three disulfide bridges is the biologically active part of the molecule affecting food intake. The C-terminal part contains half-cystine residues in positions 55, 61, 73, 75, 81, and 88, and we have previously shown that these are disulfide linked in the configuration I−III, II−V, and IV−VI when the half-cystines are numbered from the N-terminal end (*7*).

In the present study, we have applied NMR spectroscopy to determine the three-dimensional structure of the disulfide linked C-terminal part of the human CART molecule ranging from residues 48 to 89 [corresponding to the rat CART(61−102)]. Structure determination of the CART peptide may enable us to rationalize binding surfaces of the peptide and subsequently investigate the possibilities to mimic these functional epitopes with the aim to develop a compound with potential satiety-controlling ability.

MATERIALS AND METHODS

CART peptides were prepared as described previously (*7*) from the same batch used for biological assays. Two versions of the CART peptide were investigated by NMR, CART(42−89), and CART(48−89), but structurally we only describe the latter form since the N-terminal part is disordered.

Samples. NMR samples were prepared by dissolving the lyophilized protein powder in 10%/90% D_2O/H_2O to approximately 1 mM concentration and adjusting the pH to

† Coordinates have been deposited with the Protein Data Bank, accession no. 1HY9 (accessible upon publication).

* To whom correspondence should be addressed. E-mail: svl@novonordisk.com.

[1] Abbreviations: CART: cocaine and amphetamine regulated transcript, ICV: intracerebroventricular, DQF: double quantum filtered, COSY, correlated spectroscopy, TOCSY: total correlation spectroscopy, NOESY, nuclear Overhauser enhancement spectroscopy, RMS: root-mean-square.

10.1021/bi010433u CCC: $20.00
Published on Web 07/13/2001

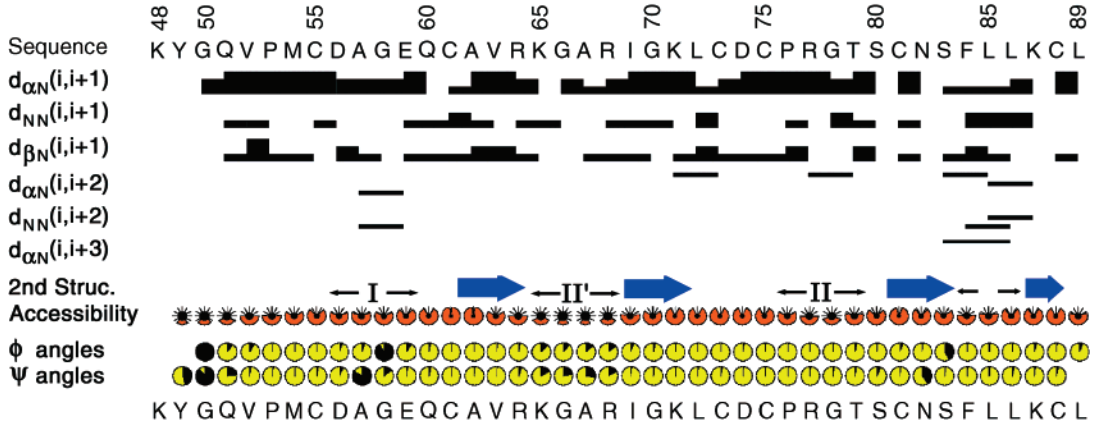

FIGURE 1: Summary of sequential NOEs (black and blue) identified from residue i to i+1 denoted $d_{ab}(i,i+1)$ with subscripts a and b indicating proton names. For proline H^{δ} NOEs are listed instead of NOEs of backbone amide protons. Secondary structure elements (2nd Struc.) are based on analysis of the ensemble of calculated structures. The β-strand elements from 80 to 82 and 87 to 88 are not present in all 10 structures. Three turns can be identified based on backbone dihedral angles and the presence of a hydrogen bond from residue i to residue i+3 in a four-residue turn. The last turn indicated from residues 84 to 86 does not belong to any classification, nor is there a hydrogen bond to stabilize the turn. Accessibility and backbone dihedral angles ϕ and ψ order parameter are directly pasted from analysis in PROCHECK. In particular, the half-cystine residues are found in the core of the protein as seen by the accessibility circles. Backbone angle order parameters show that the ϕ- and ψ-angles of Gly 50 are completely disordered. Disorder is also observed at residue positions 55−56, 65−68, and 82−83, located in turns with few NOEs to define the structure.

6.5 by addition of small volumes of 0.2 N HCl or NaOH. All pH meter readings are without correction for isotope effects. Samples in pure D_2O were prepared after three cycles of redissolving the freeze-dried powder in D_2O.

NMR. Two-dimensional ^{1}H-^{1}H NMR spectra, DQF-COSY (*8*, *9*), TOCSY (*10*, *11*), and NOESY (*12*, *13*) were recorded either at 600 MHz Unity Inova, Varian or 750 MHz Unity Inova, Varian at 300 K. For each phase sensitive two-dimensional NMR spectrum 512 t_1 increments were acquired using the States-Haberkorn method (*14*). Spectral widths of 11 ppm in both dimensions were used, with the carrier placed exactly on the water resonance which was attenuated by using saturation between scans or by using WATERGATE (*15*). Typically, 1.5 s were used for relaxation delay. For TOCSY spectra mixing times between 30 and 80 ms were used and for NOESY mixing times between 50 and 200 ms were used.

The processing of the NMR data was performed on a SGI Indigo-2 using either XWINNMR 1.3 (BRUKER), VnmrSGI 5.3b (VARIAN) or the processing package MNMR version 97.2 (PRONTO Software Development and Distribution, Copenhagen, Denmark). Prior to Fourier transformation window functions were applied, sinebells shifted $\pi/4$ in t_2 and squared sinebells shifted $\pi/2.6$ in t_1 and zero-filling performed once in each dimension.

Spectral assignments were performed assisted by the program PRONTO (*16*) (PRONTO Software Development and Distribution, Copenhagen Denmark). Chemical shifts are reported in ppm as observed relative to dioxane (3.75 ppm). The applied algorithm for measurements of $^3J_{H^NH^\alpha}$ coupling constants built into the PRONTO software package uses a combined analysis of NOESY and COSY peaks (*17*). Stereospecific assignments for side chain protons were obtained by identifying one of three staggered rotamer conformations using NOESY and a high ω_2 resolved (1.96 Hz/point) COSY (*18*). The criteria for a hydrogen bond to exist in the ensemble of calculated structures is that the CO−NH distance is less than 3.3 Å and the N−H−O angle is greater than 130° among all structures.

Structure Determination. Distance restraints for subsequent structure calculation were obtained from integrated NOESY cross-peaks classified as either weak, medium, or strong corresponding to upper distance restraints of 5.0, 3.3, and 2.7 Å, respectively, based on NOESY spectra with mixing times 100, 150, and 200 ms conservatively interpreted to avoid spin diffusion based restraints. For distance restraints involving methyl groups, an additional 0.5 Å was added to the upper limit. Disulfide pairing was determined previously (*7*) from the same batch of protein that was used in this study, and subsequently that information was used directly as NOEs in the structure calculation. ϕ-angle restraints were obtained from $^3J_{H^NH^\alpha}$ coupling constants, $-60 \pm 30°$ (2 Hz − 4 Hz), $-70 \pm 30°$ (4 − 6 Hz), $-120 \pm 60°$ (6 − 8 Hz), and $-120 \pm 35°$ (8 − 10 Hz). Structure calculations were performed by the hybrid method combining distance geometry and simulated annealing using the standard protocols (*19*, *20*) in X-PLOR (*21*). Out of 100 structures, 10 converged structures were selected for representation based on lowest energy.

Graphic Illustrations. Figures of molecules were produced using either Insight (Molecular Simulation Inc.), MOLSCRIPT (*22*) combined with RASTER3D (*23*), GRASP (*24*), or PRONTO (*16*).

RESULTS AND DISCUSSION

Structure Determination. Structure calculations of CART were based on NMR derived restraints extracted from spectra acquired at 27 °C and pH 6.5 with no extra addition of buffers and salts except from the small amount of acid and base used for pH calibration and the known pairing of half-cystines from previous studies (*7*) included initially as distance restraints. NMR spectra of CART at different concentrations in the range 0.01 to 1.0 mM showed no sign of protein aggregation.

Spin systems resonance assignments and sequential assignments were performed following the principles described by Wüthrich (*25*). Spin system assignment were straightforward for amino acids of the short peptide but minor

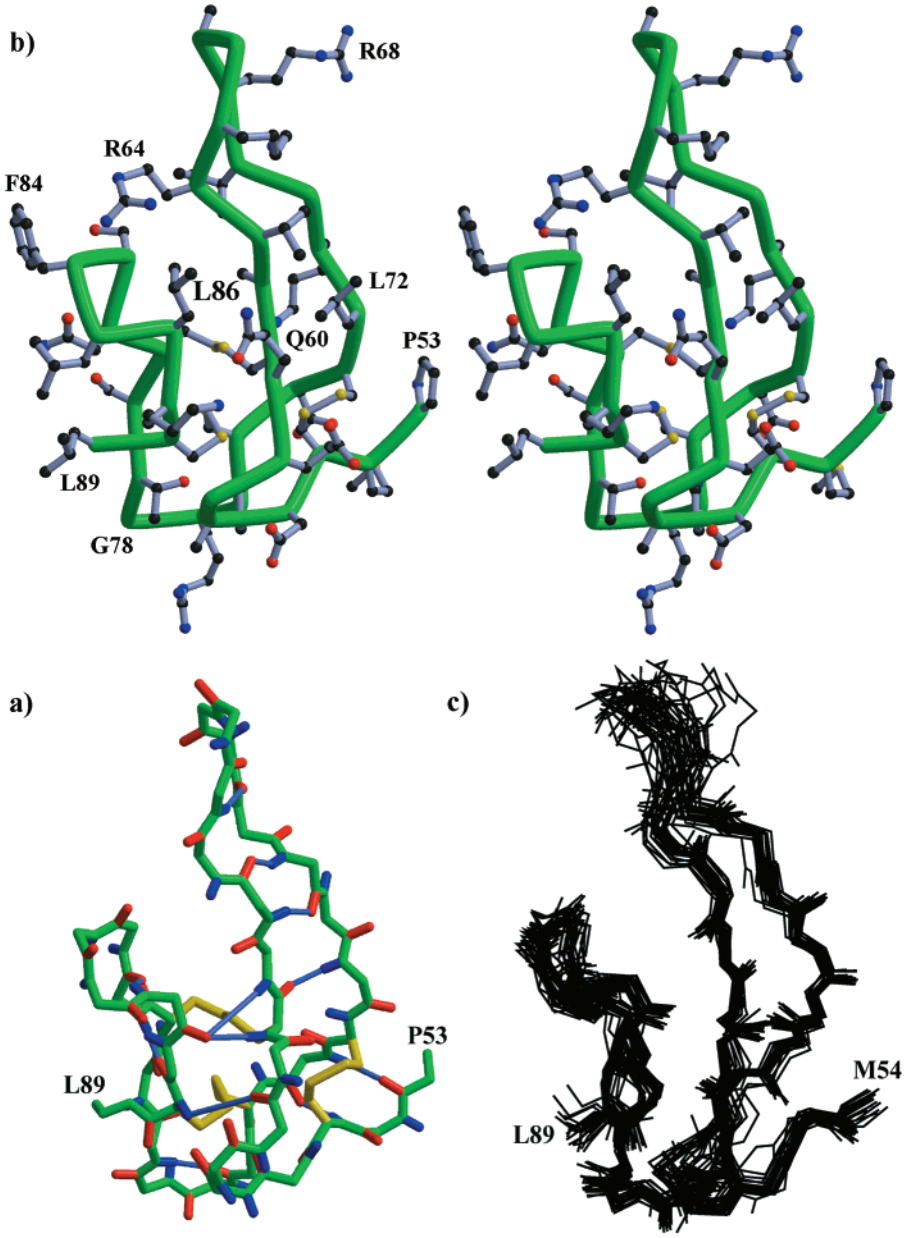

FIGURE 2: Three representations of the solution structure of CART describing several aspects of the structural arrangement. Annotations in the panels refer to residue type and sequence number. The N-terminal peptide 42−52 is disordered, and only the well-defined part of CART is shown in the panels. (a) backbone representation and disulfide bridges (yellow) of CART with hydrogen bonds in light blue between backbone amides protons and carbonyl oxygens as found in all 10 representative structures (see text). (b) Schematic wormlike backbone representation in stereo with heavy atom side chains with selected annotations, and (c) showing the ensemble of 10 structures based on NMR derived distance and torsion angle restraints. Both two upper loops are less well defined as compared to the rest of the structure.

difficulties were observed for certain residues for which the resolution of cross-peaks were poor, i.e., residues 57−58, 65−68, and 81−83. Furthermore, small fractions of the protein had oxidized methionine in position 54 (approximately 20%) resulting in two very distinct sets of spin systems for Met 54 and Asp 74 (structural neighbor to Met 54). Other residues were only slightly influenced by the fractional methionine heterogeneity. The appearance of sequential NOEs is summarized in Figure 1. Ten converged structures (Figure 2 panel c) were selected out of 100 structures based on lowest energy calculated after the simulated annealing and minimization stage. The atomic RMS between the 10 structures and their geometric average was 0.67 ± 0.19 Å and 1.13 ± 0.20 Å for backbone and heavy atoms in residues 54−89, respectively. Structural statistics describing the results of the structure calculations are given in Table 1. The quality of the structures was assessed using PROCHECK (*26*), and this analysis showed that the few residues in disallowed regions of the Ramachandran plot also were low in the number of NOE and dihedral angle restraints per residue and showed a high angular variance for backbone dihedral angles (Figure 1). The ϕ-angle of Leu 86 came out positive even in the very early stages of structure calculations in nice agreement with the 7 Hz $^{3}J_{H^{N}H^{\alpha}}$ coupling constant and the very intense intraresidual H^{N}-H^{α} NOE characteristic for positive ϕ-angles. The most favorable structure among the 10 structures analyzed in PROCHECK (equivalent resolution is 2.3 Å) is also well behaved with

Table 1: Structural Statistics of the Solution Structure of CART(48−89) at 300 K and pH 6.5 in 10%/90% D_2O/H_2O

distance restraints	633
total:	
short range ($1 \leq \|i - j\| < 5$)[a]	216
long-range intrachain	151
dihedral angle restraints:	46
ϕ	28
χ^1	14
χ^2	4

average number of all NOE restraint violations

0.0 to 0.1 Å	6.1 ± 2.0
0.1 to 0.2 Å	1.3 ± 0.9
0.2 to 0.3 Å	0.3 ± 0.5
0.3 to 0.4 Å	0.3 ± 0.6
> 0.4 Å	0
rms deviation	0.009 ± 0.003 Å

average number of dihedral restraint violations

>3°	0
rms deviation	0.21± 0.09°

deviations from idealized geometry

impropers	0.32 ± 0.03°	(0 violations above 5°)
angles	0.56 ± 0.02°	(0 violations above 5°)
bonds	0.0050 ± 0.0002 Å	(0 violations above 0.05 Å)

energies[b]	
total energy	103.5 ± 11.6
bond	16.5 ± 1.1
angle	52.6 ± 2.9
improper	4.7 ± 1.0
repel	26.4 ± 10.2
NOE	3.0 ± 1.8
torsion	0.2 ± 0.1
VdW[c]	−135.1 ± 4.7

atomic root-mean-square values for 10 calculated structures versus average coordinates:

atoms included	rms [Å]
backbone (54−89)	0.67 ± 0.19
heavy atoms (54−89)	1.13 ± 0.20
backbone (54−63,68−89)	0.53 ± 0.12
heavy atoms (54−63,68−89)	0.88 ± 0.15

PROCHECK Ramachandran plot statistics (residues 52−66, 69−81, 84−85,87−89)

residues in most favoured regions	73.8%
residues in additional allowed regions	26.0%
residues in generously allowed regions	0.2%
residues in disallowed regions	0.0%

[a] Ranges are defined between residues i and j in the sequence within one chain. [b] Energies (kcal mol^{-1}), measured with simplified repel potential used in the simulated annealing protocol, $k_{NOE} = 50$ kcal mol^{-1} $Å^{-2}$, $k_{tor} = 200$ kcal mol^{-1} rad^{-2}, $k_{impr} = 500$ kcal mol^{-1} rad^{-2}, $k_{bond} = 1000$ kcal mol^{-1} $Å^{-2}$, $k_{ang} = 500$ kcal mol^{-1} rad^{-2}, and $k_{repel} = 4$ kcal mol^{-1} rad^{-2} (vdw radii set 0.80 relative to normal values). [c] Van der Waal energy measured with CHARMM potential.

respect to satisfy the distance and dihedral angle restraints and the energy target function. This structure was chosen as the representative structure.

The set of distance and dihedral angle restraints obtained were sufficient to obtain a reasonable converged set of structures. Two factors have in this case a negative influence on the quality of the structure: first, spin systems from residues 57−58, 65−68, and 81−83 consist of poorly resolved cross-peaks and are only involved in few inter-residual interactions observed as NOEs typically as a result of conformational exchange on the intermediate time scale, and second, a minor fraction of oxidized Met-54 prevents NOEs from being correctly interpreted with respect to intensity and subsequently restraint range.

Description of the Structure. The secondary structure of the 42-amino acid peptide CART is shown in Figure 2. Three turns are identified: type I turn, 56−59 (preferential classification among the 10 structures); type II′ turn 65−68; and type II turn 76−79. The most prominent regular secondary structural element is the short antiparallel β-sheet including residues 62−64 and 69−71 but additionally a second very short antiparallel β-sheet could be identified spanning residues 81−82 and 87−88. All the turns and sheets described have the required hydrogen bonds. On the basis of the 10 structures, we can list the following hydrogen bonds between backbone amides and carbonyls, H^N55-O61, H^N59-O56, H^N61-O86, H^N63-O70, H^N65-O68, H^N68-O65, H^N70-O63, H^N72-O61, H^N74-O53, H^N79-O76, H^N82-O87, H^N88-O59, and H^N89-O80, all except the last one shown in Figure 2 panel a, also consistent with slow exchange of the included amide protons as observed in a NOESY spectrum recorded of freshly dissolved CART peptide in near 100% D_2O. All the mentioned hydrogen bonds were not included at any stage as distance restraints in the structure calculations. Hydrogen bonds involving side chain donors/acceptors are less well defined, but a few appears in most of the ensemble of structures, Glu 59 H^N to Asp 56 O^δ, Gln 60 H^ϵ to Ala 62 C−O, Thr 79 H^γ to Pro 76 C−O, and Lys 87 H^ζ to Glu 59 C−O and charge interactions Lys 71 H^ζ to Asp 74 O^δ, identified only from the structural data.

Among the most buried residues, we find all the cystines and in particular Ala 62, which is surrounded by residues 61, 69−71, 81, 83, and 86 and thus represents the central core of the protein. A cluster of positively charged residues are exposed on the surface of CART by residues Arg 64, Lys 65, and Arg 68. A relatively large number of hydrophobic residues are also exposed on the surface of CART in a large continuous surface composed by residues Leu 85, Leu 86, and Leu 89 and Phe 84, which again is neighbored by a smaller hydrophobic surface exposed area consisting of residues Pro 53, Val 52, Met 54, Val 63, and Leu 72.

Structural Homology to Cystine Knots. The fold of the C-terminal CART peptide belongs to the fold-family of small globular knottins (*27*) or cystine knot structures (*28*) including agatoxins, conotoxins, versutoxins, cellulose binding domains, and gurmarin consisting of 25−50 amino acid residues.

These peptides are small peptides and without other structural elements than those described in CART. In contrast to the lack of sequence homology, the existing structural homology was analyzed partly using FSSP/DALI (*29*) or by manual inspection of structures, and a sequence alignment could be constructed (Figure 3). The sequence alignment based on equal structure folds could ultimately pinpoint certain structural key residues that could help us to understand the structure better and subsequently to rationalize the key residues of structural importance and those of potential functional interest. Residues 56−61, 74−75, 79−83, and 86−89 (shown in blue) in Figure 3 are used for aligning the structures, and the atomic RMS values between any two structures for regions drawn in blue are in all cases below 1.0 Å for backbone atoms. These residues seem to display a common framework which several proteins have applied, and on this framework different length of loops and turns are added to achieve the desired functionality of the peptide.

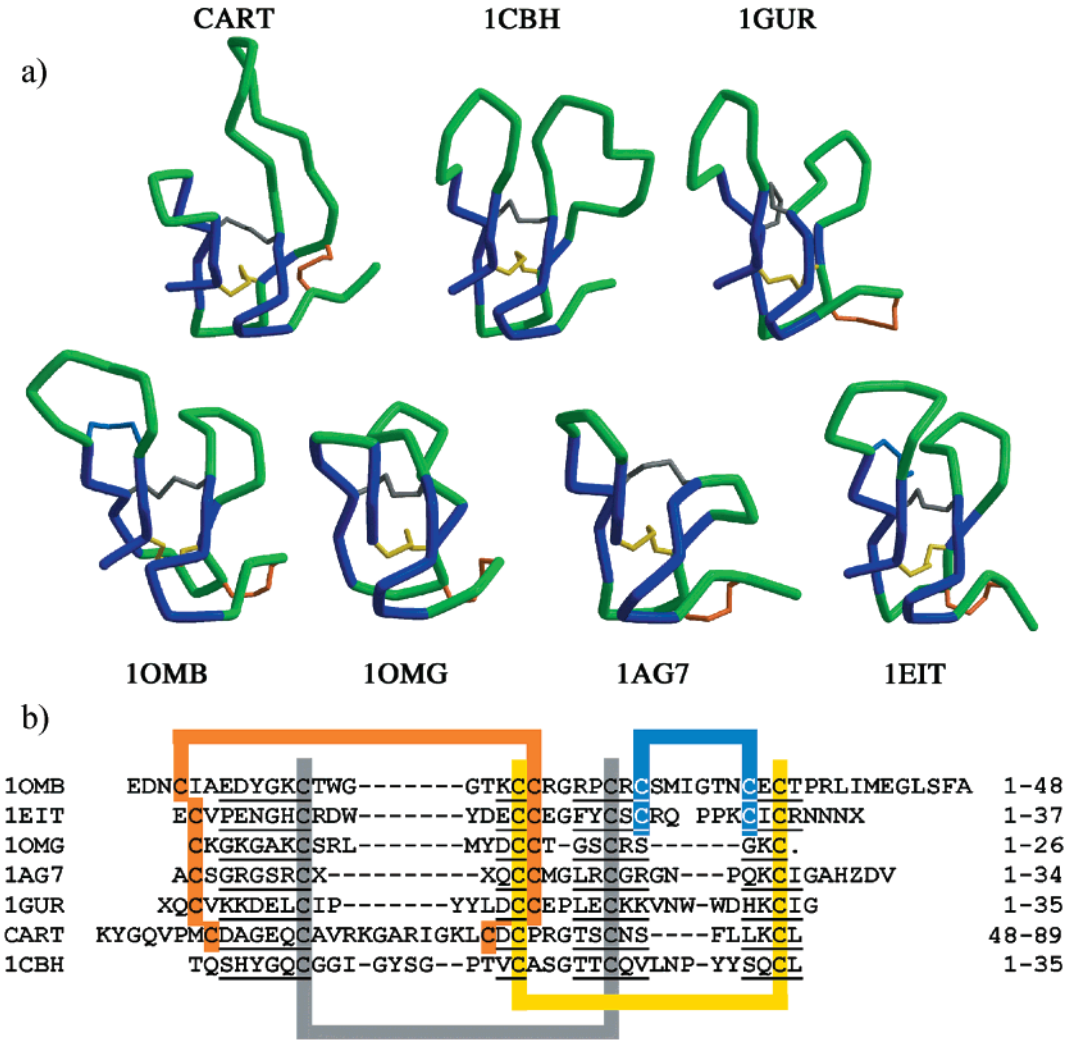

FIGURE 3: (a) Seven protein structures in backbone representation all based on the same general fold with variations in loop sizes and number of disulfide bridges. The structures are annotated with their respective Brookhaven id code, except CART. The blue part of the backbones is a common fold used for alignment in all structures with atomic RMS values less than 1.0 Å. The colors of the disulfide bridges refer to colors of the bars behind Cys residues in panel b. In panel b the seven protein structures are aligned based on structural homology as illustrated in panel a), and the underlined residue positions correspond to the blue regions of the backbones in panel a). The seven structures are each representatives of the various families of structures, which include even more structures. The abbreviations refer directly to PDB id codes. 1OMB, a ω-agatoxin from a spider, *Agelenopsis aperta* (*33*); 1EIT, a μ-agatoxin-I from spider, *A. aperta* (*34*); 1OMG, an ω-conotoxin M VIIa from seasnail *Conus magus* (*35*); 1AG7, conotoxin GS from seasnail *C. Geographus* (*36*); 1GUR, gurmarin a sweet taste-suppressing protein from the leaves of *Gymnema sylvestre* (*37*); CART (pdb code1HY9), cocaine and amphetamine regulated transcript peptide from human; and 1CBH, celloluse binding domain (C-terminal domain) of cellobiohydrolase I from *Trichoderma Reesei* (*38*). Additional PDB entries with similar fold are 1C4E (*39*), 1AGG (*40*), 1OAV (*41*), 2CCO (*42*), 1OMC (*43*), 1MVJ (*44*), 1OMN (*45*), and 1MVI (*44*).

Disulfide Bridge Pairing. The pairing of half-cystines to disulfide bridges in CART is I−III, II−V, and IV−VI different from the pairing in the other structures in Figure 3, which are I−IV, II−V, and III−VI, but still the structural alignment is obvious. It is clear from Figure 3 that the disulfide bridge I−III (in CART) or I−IV (in all the others), is structurally equivalent and supports the common structural fold. A search for peptides with approximately the same size and the same disulfide bridge pairing (I−III, II−V, and IV−VI) as CART in the Brookhaven protein structure database identified among others a number of structures including 1ldl, low-density lipoprotein receptor first repeat, 1ldr, low-density lipoprotein receptor second repeat, and 1ajj, low-density lipoprotein receptor fifth repeat. Although the half-cystine paring among these was the same, these structures turned out to have a clearly different fold from CART. Among the disulfides bridges, the gray (I−IV) and the yellow (III−VI) ones are the most fundamental ones since these are those that are generally repeated among the peptides with a common structural framework (*30*).

Structural Epitopes. Besides the shared structural framework of CART and the cystine knots, CART differs from the other structures with respect to loops and turns, in particular the loop spanning residues 64−69 which is the largest among the seven, whereas the other loop or merely a turn, including residues 84−86, is the shortest among the peptides illustrated in Figure 3. The relatively large hydrophobic areas exposed on the surface of CART apparently had no impact on a potential aggregating surface of the peptide at least at the 1 mM concentrations used for NMR since no sign of aggregation was observed. Without other data to substantiate any structural epitopes, the large hydrophobic surface presented by residues Leu 85, Leu 86, Leu 89, and Phe 84 could thus be a potential hot spot for a

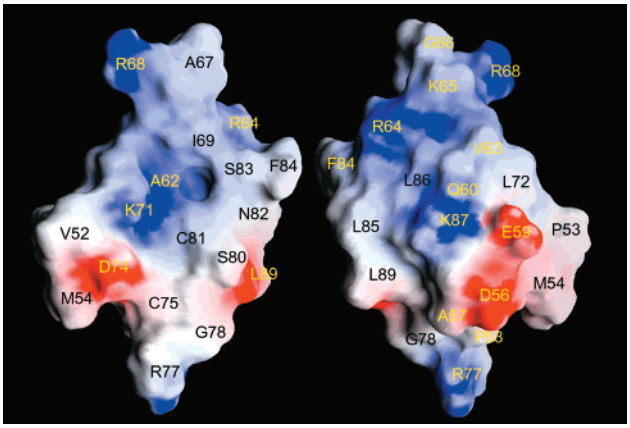

FIGURE 4: GRASP surface models of CART from the front and the back of the molecule. The right side presents a view of the molecule as seen in Figure 2. Blue colored surfaces represent positively charged areas, red surfaces represent negatively charged areas, and white surfaces represent neutral areas. Color intensities are produced according to maximum blue or red color intensity at $\pm$ 10 k_BT (where k_B and T are the Boltzmann constant and temperature, respectively).

possible receptor interaction, whereas the cluster of charged residues, Arg 64, Lys 65, and Arg 68, appears to have a more functional task possibly enhancing solubility or facilitating active membrane crossing capability. Surfaces colored by electrostatic potentials (Figure 4) using GRASP (*24*) are dominated by the positive charges from the previous mentioned basic residues. Lysines are usually located on the surface of proteins; however, Lys 71 has a dense network of NOEs to its structural neighbors could indicate that this special location of a charge residue plays a central role in the formation of a positively charge pocket which appears as a like site for a possible binding pocket either as part of a receptor binding recognition site or anion binding site. All side chain protons in Lys 71 including the H^{ϵ} group have an extensive NOE network to the surrounding residues indicating that this side chain is not freely rotating on the surface but has been structurally restrained. CART(49−63) has been reported to have an inhibitory effect on the food intake in goldfish (*31*) (named CART(62−76) according to the long form without signal peptide) and CART(42−63) in rat (*32*) (named CART(82−103) according to the long form in rat including the signal peptide) but a reduced effect relative to CART(49−89). As compared to our structure, these peptides have an unordered N-terminal until Cys 55 followed by a type I turn (56−59), Cys 61, and a small stretch of β-strand (62−63). It is not clear from the two reports if the peptides have disulfide linkage between Cys 55 and Cys 61. In CART(49−89), this linkage is not formed, but structurally little should change in the two peptides to allow this disulfide bridge to form and still maintain the original conformation of the central portion of the peptide.

ACKNOWLEDGMENT

We thank Svend Hastrup, Asser Andersen, Michi Egel-Mitani, and Ivan Diers for cDNA constructions of CART and fermentation, and the "Danish Instrument Center for NMR spectroscopy of Biological Macromolecules" for access time to the 750 MHz NMR instrument.

SUPPORTING INFORMATION AVAILABLE

^{1}H NMR assignments obtained for the human CART(48−89) and the six N-terminal linked residues belonging to CART(42−89). This material is available free of charge via the Internet at http://pubs.acs.org.

REFERENCES

1. Kristensen, P., Judge, M. E., Thim, L., Ribel, U., Christjansen, K. N., Wulff, B. S., Clausen, J. T., Jensen, P. B., Madsen, O. D., Vrang, N., Larsen, P. J., and Hastrup, S. (1998) *Nature 393*, 72−76.
2. Campfield, L. A., Smith, F. J., and Burn, P. (1998) *Science 280*, 1383−1387.
3. Douglass, J., Mckinzie, A. A., and Couceyro, P. (1995) *J. Neurosci. 15*, 2471−2481.
4. Douglass, J., and Daoud, S. (1996) *Gene 169*, 241−245.
5. Thim, L., Kristensen, P., Nielsen, P. F., Wulff, B. S., and Clausen, J. T. (1999) *Proc. Natl. Acad. Sci. U.S.A. 96*, 2722−2727.
6. Spiess, J., Villarreal, J., and Vale, W. (1981) *Biochemistry 20*, 1982−1988.
7. Thim, L., Nielsen, P. F., Judge, M. E., Andersen, A. S., Diers, I., Egel-Mitani, M., and Hastrup, S. (1998) *FEBS Lett. 428*, 263−268.
8. Piantini, U., Sørensen, O. W., and Ernst, R. R. (1982) *J. Am. Chem. Soc. 104*, 6800−6801.
9. Rance, M., Sorensen, O. W., Bodenhausen, G., Wagner, G., Ernst, R. R., and Wuthrich, K. (1983) *Biochem. Biophys. Res. Commun. 117*, 479−485.
10. Bax, A., and Davis, D. G. (1985) *J. Magn. Reson. 65*, 355−360.
11. Braunschweiler, L., and Ernst, R. R. (1983) *J. Magn. Reson. 53*, 521−528.
12. Jeener, J., Meier, B. H., Bachmann, P., and Ernst, R. R. (1979) *J. Chem. Phys. 71*, 4546−4553.
13. Kumar, A., Wagner, G., Ernst, R. R., and Wuthrich, K. (1981) *J. Am. Chem. Soc. 103*, 3654−3658.
14. States, D. J., Haberkorn, R. A., and Ruben, D. J. (1982) *J. Magn. Reson. 48*, 286−292.
15. Piotto, M., Saudek, V., and Sklenar, V. (1992) *J. Biomol. NMR 2*, 661−665.
16. Kjaer, M., Andersen, K. V., Shen, H., Ludvigsen, S., Windekilde, D., Sørensen, B., and Poulsen, F. M. (1991) in *NATO ASI Series* (Hoch, J. C., Redfield, C., and Poulsen, F. M., Eds.) Plenum, New York.
17. Ludvigsen, S., Andersen, K. V., and Poulsen, F. M. (1991) *J. Mol. Biol. 217*, 731−736.
18. Hyberts, S. G., Märki, W., and Wagner, G. (1987) *Eur. J. Biochem. 164*, 625−635.
19. Kuszewski, J., Nilges, M., and Brünger, A. T. (1992) *J. Biomol. NMR 2*, 33−56.
20. Nilges, M., Clore, G. M., and Gronenborn, A. M. (1988) *FEBS Lett. 229*, 317−324.
21. Brünger, A. T. (1993) X-PLOR Version 3.1: A System for X-ray Crystallography and NMR [3.851], Yale University Press, New Haven, CT.
22. Kraulis, P. J. (1991) *J. Appl. Crystallogr. 24*, 946−950.
23. Merritt, E. A., and Murphy, M. E. (1994) *Acta Crystallogr. Sect. D Biol. Crystallogr. 50*, 869−873.
24. Nicholls, A., Sharp, K. A., and Honig, B. (1991) *Proteins 11*, 281−296.
25. Wuthrich, K. (1986) *NMR of Proteins and Nucleic Acids*; John Wiley, New York.
26. Laskowski, R. A., Rullmann, J. A., Macarthur, M. W., Kaptein, R., and Thornton, J. M. (1996) *J. Biomol. NMR 8*, 477−486.
27. Murzin, A. G., Brenner, S. E., Hubbard, T., and Chothia, C. (1995) *J. Mol. Biol. 247*, 536−540.
28. Norton, R. S., and Pallaghy, P. K. (1998) *Toxicon 36*, 1573−1583.
29. Holm, L., and Sander, C. (1998) *Nucleic Acids Res. 26*, 316−319.

30. Flinn, J. P., Pallaghy, P. K., Lew, M. J., Murphy, R., Angus, J. A., and Norton, R. S. (1999) *Biochim. Biophys. Acta 1434*, 177−190.
31. Volkoff, H., and Peter, R. E. (2000) *Brain Res. 887*, 125−133.
32. Lambert, P. D., Couceyro, P. R., McGirr, K. M., Dall-Vechia, S. E., Smith, Y., and Kuhar, M. J. (1998) *Synapse 29*, 293−298.
33. Yu, H., Rosen, M. K., Saccomano, N. A., Phillips, D., Volkmann, R. A., and Schreiber, S. L. (1993) *Biochemistry 32*, 13123−13129.
34. Omecinsky, D. O., Holub, K. E., Adams, M. E., and Reily, M. D. (1996) *Biochemistry 35*, 2836−2844.
35. Kohno, T., Kim, J. I., Kobayashi, K., Kodera, Y., Maeda, T., and Sato, K. (1995) *Biochemistry 34*, 10256−10265.
36. Hill, J. M., Alewood, P. F., and Craik, D. J. (1997) *Structure 5*, 571−583.
37. Arai, K., Ishima, R., Morikawa, S., Miyasaka, A., Imoto, T., Yoshimura, S., Aimoto, S., and Akasaka, K. (1995) *J. Biomol. NMR 5*, 297−305.
38. Kraulis, J., Clore, G. M., Nilges, M., Jones, T. A., Pettersson, G., Knowles, J., and Gronenborn, A. M. (1989) *Biochemistry 28*, 7241−7257.
39. Fletcher, J. I., Dingley, A. J., Smith, R., Connor, M., Christie, M. J., and King, G. F. (1999) *Eur. J. Biochem. 264*, 525−533.
40. Reily, M. D., Thanabal, V., and Adams, M. E. (1995) *J. Biomol. NMR 5*, 122−132.
41. Kim, J. I., Konishi, S., Iwai, H., Kohno, T., Gouda, H., Shimada, I., Sato, K., and Arata, Y. (1995) *J. Mol. Biol. 250*, 659−671.
42. Pallaghy, P. K., and Norton, R. S. (1999) *J. Pept. Res. 53*, 343−351.
43. Davis, J. H., Bradley, E. K., Miljanich, G. P., Nadasdi, L., Ramachandran, J., and Basus, V. J. (1993) *Biochemistry 32*, 7396−7405.
44. Nielsen, K. J., Thomas, L., Lewis, R. J., Alewood, P. F., and Craik, D. J. (1996) *J. Mol. Biol. 263*, 297−310.
45. Farr-Jones, S., Miljanich, G. P., Nadasdi, L., Ramachandran, J., and Basus, V. J. (1995) *J. Mol. Biol. 248*, 106−124.

BI010433U